Final Report: DE-SC0002000
"Winter storms and the Spring Transition over the western U.S.: Quantifying discrepancies between coarse and high-resolution simulations and observations"
Miller, Cayan and Pierce (SIO, UCSD)

a. Research accomplishments

This project addressed the ability of the Community Climate System Model (CCSM3 and CCSM4), the Community Earth System Model (CESM), and other models to simulate the processes involved in controlling winter storms affecting the U.S. West Coast as well as other precipitation processes in the climate system.

i. CCSM4 precipitation statistics in the western U.S.

Water resources have extensive influence on government policy, quality of life, and regional economics. This is particularly true over the western U.S., which harbors a rapidly growing population, very active climate variability and a complex topography that affects regional climate including the spatial and temporal structure of precipitation. The generally arid southwestern U.S., which is the fastest growing region of the United States, is one area where effective water management is of paramount importance. The Pacific Northwest lies in the influence of interannual and interdecadal climate variation. In addition, flooding has major impacts in the region, and is a major player in regional economic policy, particularly in California. For example, in 2010, the Federal Emergency Management Agency forced homeowners in Los Angeles, Orange, Ventura, Riverside, and San Bernardino counties to buy flood insurance because of their proximity to flood-prone rivers and creeks.

Synoptic weather patterns over the western U.S. are known to be influenced by the El Niño-Southern Oscillation (ENSO) and the Pacific Decadal Oscillation (PDO). The teleconnected signal of ENSO in climatic variables across the globe has been an important topic of research for many decades. Many coupled GCMs have exhibited unrealistic teleconnections between ENSO fluctuations and extratropical circulation patterns, driven in part from having poorly represented physical processes in the core ENSO region. The warm and cool phases of the PDO are also associated with distinctly different western U.S. weather patterns, despite the lack of robust evidence for physical causality of decadal North Pacific SST variability.

DeFlorio et al. (2012) assessed the NCAR Community Climate System Model, version 4 (henceforth CCSM4) skill in simulating several teleconnected signals of ENSO and the PDO over the North Pacific, extreme regional precipitation over the western U.S. and North Pacific, and the relationship of the phase of both ENSO and the PDO to western U.S. extreme precipitation. We also compared CCSM4 to results from CCSM3 (the previous version of the model), observations, and reanalysis.

Fig. 1 shows the seasonal climatology of mean precipitation for the Hamlet and Lettenmaier data set compared to both CCSM3 monthly data at T85 (~1.4°) resolution and CCSM4 daily data at ~1.25° lat x 0.9° lon resolution. It is clear that climatological precipitation is more realistic in CCSM4, both in spatial structure and seasonal agreement with observations. Some of this improvement may be due to the slightly finer grid used

by CCSM4 compared to CCSM3. In particular, CCSM4 does a better job simulating the magnitude and spatial structure of several important features during the wet (September thru February) season, including the large Pacific Northwest/northern California zonal gradient in precipitation and the circular “bullseye” pattern of enhanced precipitation over north-central Idaho. The former feature can be attributed to the presence of the Cascade Mountains and northern Sierra Nevada; the latter feature is likely due to large height gradients caused by the meeting of the Snake River Plain and the Salmon River Mountains. Thus, CCSM4 demonstrates regional dexterity in simulating orographically enhanced precipitation across the domain. In comparison, CCSM4’s predecessor, CCSM3, smeared the Pacific Northwest precipitation gradient over a wide region and was unable to capture the complex precipitation response over central Idaho. One deficiency in CCSM4’s simulation is that it is drier than observations over the Pacific Northwest by several mm/day during the winter.

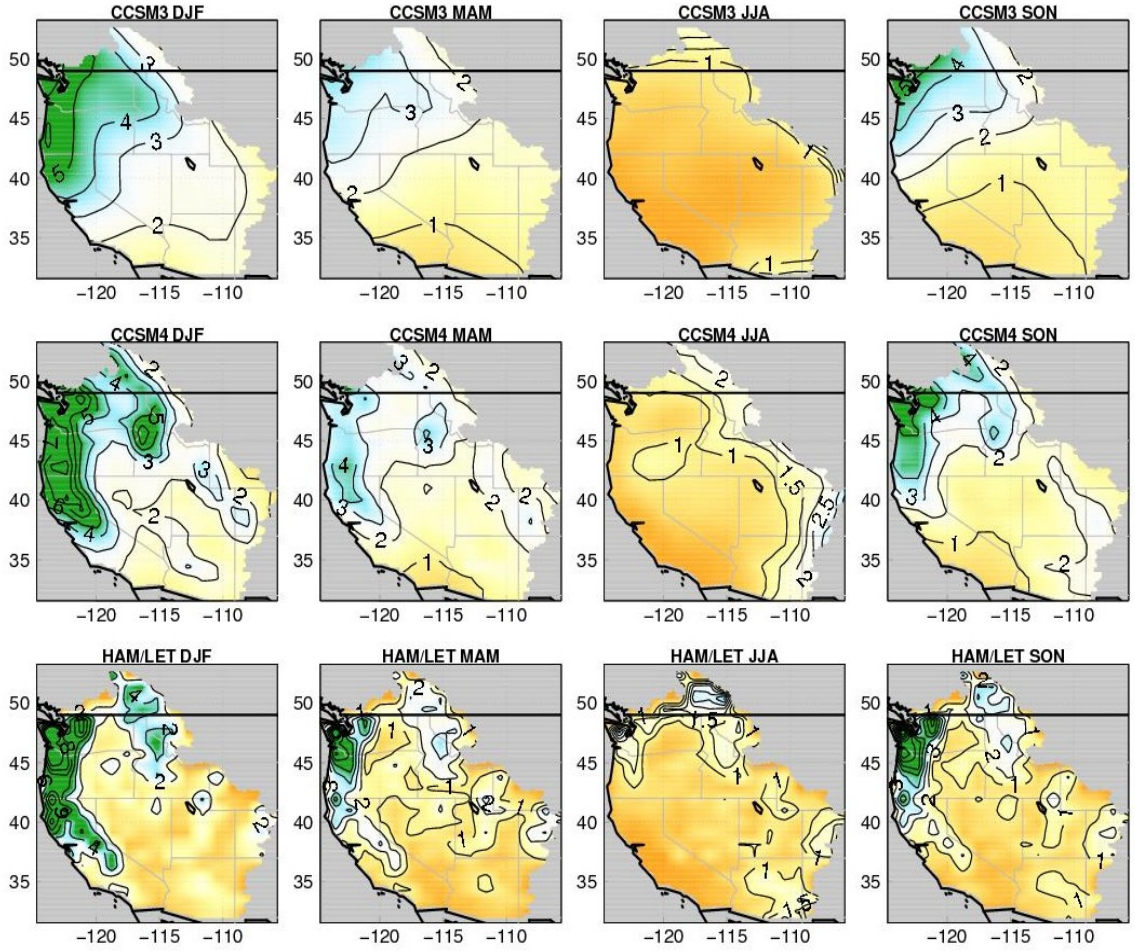

Figure 1. Seasonal climatology of precipitation (mm/day) for CCSM3, CCSM4 and observations; contour intervals are every 1 mm/day. CCSM4 shows improvement in capturing the strong observed zonal gradient in precipitation over the western U.S. (From DeFlorio et al., 2012)

Fig. 2 shows the 90th percentile value of precipitation intensity in mm/day, by season, for CCSM3, CCSM4, and observations. The calculation is made by averaging 90th percentile values for individual seasons, rather than choosing the 90th percentile value of the entire precipitation distribution. Choosing the former result is more robust, as the latter result could be skewed by a single extreme outlying year. CCSM4 adeptly simulates the wet tail (i.e. 90th percentile) of the precipitation distribution across the entire domain. Notably, during wet seasons, precipitation is most intense in north-central California, but has the greatest accumulation in the Pacific Northwest. The spatial displacement between precipitation intensity and accumulation manifests itself in the observations, and CCSM4 captures this feature quite well.

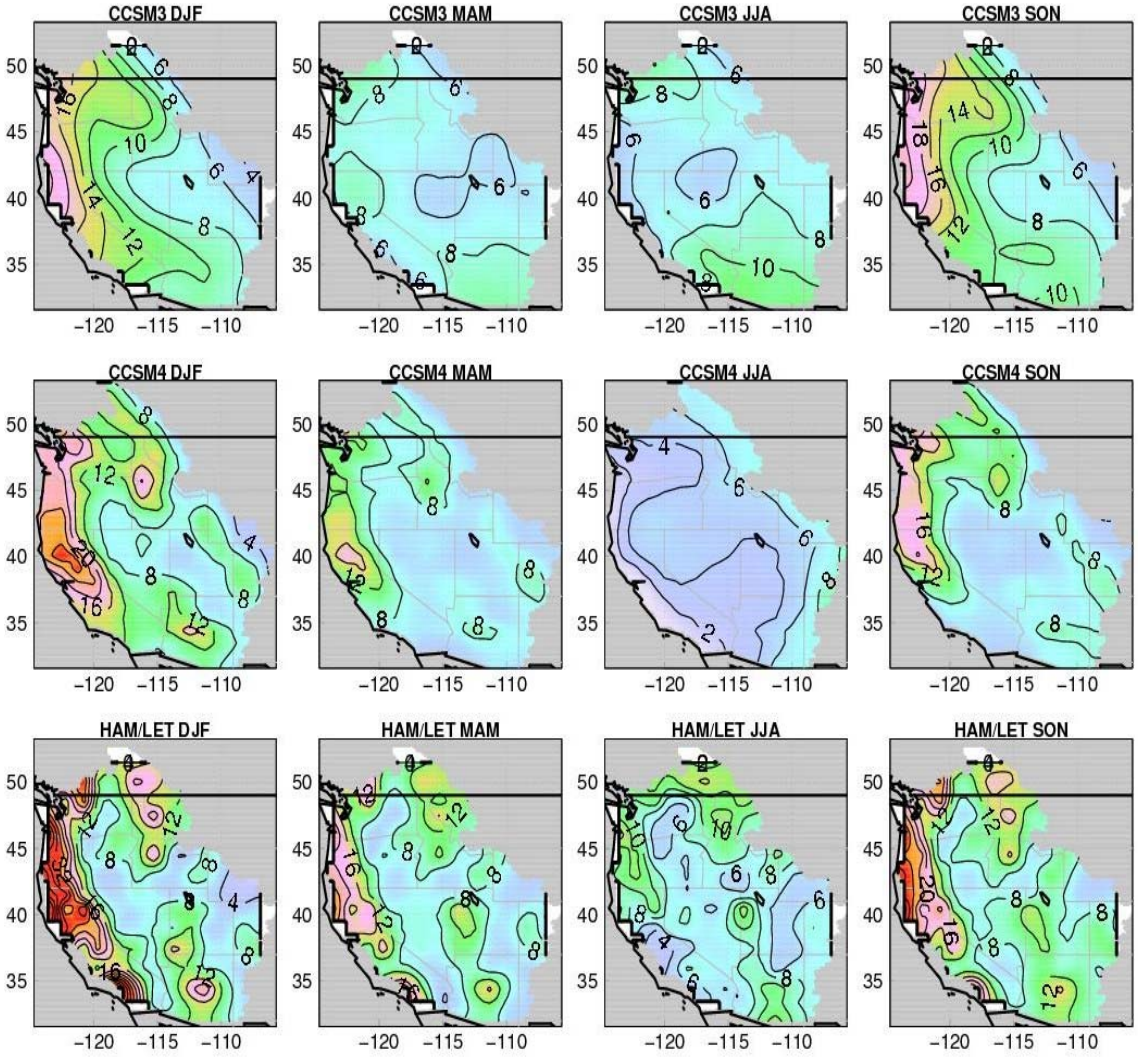

Figure 2. 90th percentile plot of precipitation intensity (mm/day) for CCSM3, CCSM4, and observations; contour labels are every 4 mm/day. CCSM4 captures observed extreme intensity events over the Sierra Nevadas, western Idaho, and central Arizona which were less resolved in CCSM3. (From DeFlorio et al., 2012)

To investigate the effect of ENSO and the PDO on extreme weather statistics, we composite extreme (90^{th} percentile) wintertime (NDJFM) precipitation intensity on wintertime seasons when the NDJFM ENSO index (top panel) or NDJFM PDO index (bottom panel) is warm (leading PC > 0.75) or cool (leading PC < -0.75). Here, the PC is standardized and is thus unitless. Note that this analysis differs slightly from those used in section 3.3 in that 90^{th} percentile precipitation intensity is calculated for each season (as before); those seasonal values then are composited on warm (leading PC > 0.75) and cool (leading PC < 0.75) ENSO/PDO seasons and averaged.

Fig. 3 shows the difference between mean 90^{th} percentile values of NDJFM precipitation intensity (mm/day) composited on warm and cool NDJFM ENSO (top panel) and NDJFM PDO (bottom panel) seasons. Differences significant at the 1σ and 2σ ($p < 0.32$ and $p < 0.05$) levels are shown as dark and light grey shading, respectively. CCSM4 is shown in the left column, while observations are shown in the right column. Fig. 3 shows that 90^{th} percentile precipitation events in the cool season are stronger over the southwest during warm ENSO seasons than during cool ENSO seasons; the opposite is true over the Pacific Northwest. This is roughly consistent with model results that show that warm ENSO conditions are prevalent during extreme wet periods over the southwest, and vice versa during extreme dry periods. Fig. 3 also shows that CCSM4 overestimates the magnitude of extreme precipitation events during warm and cool NDJFM ENSO seasons. This overestimation is less prevalent during warm and cool NDJFM PDO seasons. The results demonstrate the relationship in CCSM4 between the phase of ENSO (and to a lesser degree, the PDO) and extreme precipitation statistics over the western U.S., and underscore the model's exaggeration of this relationship compared to observations.

Extending prior work evaluating GCM simulations of ENSO and PDO teleconnections and regional precipitation events to CCSM4 is timely, since the model was released recently and will be used in the upcoming fifth IPCC assessment, and is important to the applications noted above. The model's simulation of interannual climatic variability, as captured in the frequency of ENSO events, is more realistic than that of its predecessor, CCSM3; however, the magnitude of these events is too large compared to observations. The improvement in the frequency of ENSO events is primarily due to improvements in the atmospheric convection parameterization scheme. Better parameterizations of cloud physics and atmospheric radiation have also improved simulations of precipitation type and amount. Given these improvements in simulation of large-scale decadal coupled ocean/atmospheric processes, which have significant impacts on the strength, frequency, and location of midlatitude synoptic storms, and in small-scale moisture microphysics, it is reasonable to consider the model as a viable candidate for realistically simulating global ENSO and PDO teleconnection patterns and extreme regional precipitation events.

This study builds on prior works by investigating CCSM4's representation of mean and extreme precipitation events and ENSO and PDO teleconnections, with a focus on the western U.S. and North Pacific. Besides comparing to observations, many of the CCSM4 results are compared to simulations by its predecessor CCSM3. We demonstrate that, in comparison to CCSM3, the newer CCSM4 version of the United States Community Climate Model produces improved simulations of both regional, synoptic

precipitation events over the western U.S. and tropical pacific (ENSO) and North Pacific (PDO) teleconnections to western U.S. precipitation.

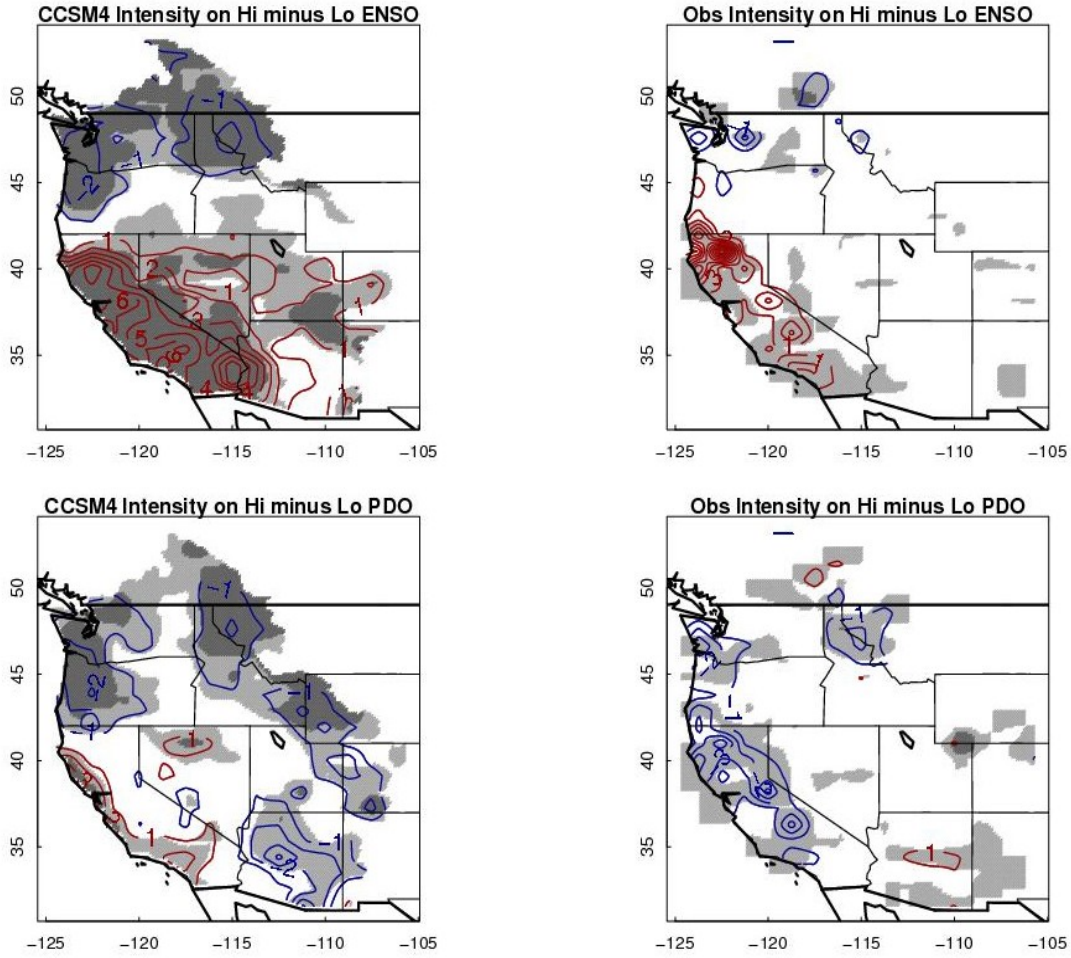

Figure 3. Difference (warm minus cool) of mean 90th percentile value of NDJFM precipitation intensity (mm/day) on warm (leading PC > 0.75) and cool (leading PC <-0.75) NDJFM ENSO (top panel) and PDO (bottom panel) years, with 95% (dark gray) and 68% (light gray) confidence intervals shaded. Positive values are indicated by red contours, indicating that 90th percentile precipitation intensity values are higher on warm NDJFM seasons than on cool seasons; the opposite is true for negative values, indicated by blue contours. CCSM4 is shown in the left column, while observations are shown on the right column. For ENSO, heavy wintertime (DJF) precipitation intensity in CCSM4 is significantly stronger over California and southern Nevada during warm ENSO years than in cool ENSO years, and the response is stronger than in observations. For the PDO, a similar qualitative pattern to ENSO years exists in CCSM4, but it is weaker. The observations show a weakly opposite pattern. Composites of precipitation duration (not shown) are quite neutral on warm and cool ENSO and PDO years. (From DeFlorio et al., 2012)

ii. Heavy precipitation and model disagreement in future climate scenarios

Climate model simulations disagree on whether annual precipitation will increase or decrease over California in the future, which has impeded efforts to anticipate and adapt to human-induced climate change. The origins of this disagreement are explored by Pierce et al. (2012) in terms of daily precipitation frequency and intensity. It is found that divergent model projections of changes in the incidence of rare heavy (> 60 mm/day) daily precipitation events explain much of the model disagreement on annual timescales, although they represent only 0.3% of precipitating days and 9% of annual precipitation volume. These results are obtained from sixteen global general circulation models downscaled with different combinations of three dynamical methods (WRF, RSM, and RegCM3) and two statistical methods (BCSD and BCCA), although not all downscaling methods were applied to each global model.

Of the 25 model projections, 22 agree that precipitation frequency will decrease by the 2060s, with a mean reduction of 6-14 days/year. This reduces California's mean annual precipitation by about 5.8%. Partly offsetting this, 19 of the 25 projections agree that daily precipitation intensity will increase, which accounts for a model average 5.2% increase in annual precipitation. Between these two conflicting tendencies, 12 projections show drier annual conditions in the state by the 2060s and 13 show wetter. Model disagreements in the projected change in occurrence of the heaviest precipitation days (> 60 mm/day) account for the majority of disagreement in the projected change in annual precipitation; when such events are excluded, nearly twice as many projections show drying as show wetter conditions.

The overall effect of seasonal changes in daily precipitation intensity and frequency is shown in Fig. 4. Equivalent changes in seasonal precipitation (cm) are calculated as in section 3.4, and results averaged across all model projections. Each region's change in future precipitation (leftmost bars in Fig. 4, green for wet and brown for dry) is equal to the sum of changes due to the number of precipitating days (middle bars in Fig. 4, yellow for less and grey for more) and precipitation intensity (rightmost bars in Fig. 4, red for greater and blue for less).

Almost all locations and seasons show an increase in daily precipitation intensity, except for winter in the south of the state. At the same time, almost all locations and seasons show a decrease in the number of precipitating days, except for the southeastern part of the state in summer. The way these two opposing tendencies combine yields a complex pattern of seasonal precipitation changes. In the northern part of the state in winter, the increase in storm intensity is stronger than the decrease in number of precipitating days, resulting in an overall mild (3-6%) increase in seasonal precipitation. In spring (MAM) a mild increase in daily precipitation intensity coupled with a strong decrease in number of precipitating days yields a significant tendency towards less precipitation (declines of > 10%). This can also be seen in autumn (SON), although the changes in storm intensity are small in this season. Finally, the southeastern part of California, on the edge of the region affected by the North American monsoon, shows both a mild increase in storm intensity and strong increase in number of precipitating days in summer (JJA), resulting in large (> 100%) increases in that season's precipitation.

Figure 4. Apportioning the seasonal precipitation change in each region to changes in storm frequency and intensity. In each set of three bars, the left most (marked "P") shows the change in precipitation during that season (cm). (For comparison, the change in seasonal precipitation is shown at the bottom of each subpanel, in percent.) This bar is colored green for positive (wetter future) changes, and brown for negative (drier future) changes. The middle bar ("Z") shows the change in seasonal precipitation (cm) that arises due to the change in number of zero-precipitation days. Yellow indicates an increase in zero precipitation days, and grey indicates a decrease. The rightmost bar (marked "I") shows the change in seasonal precipitation (cm) that arises from the change in precipitation intensity. Red shows an increasing intensity, blue shows decreasing intensity. Note that the Y=axis varies by region, but for each region is the same across all seasons. (From Pierce at al., 2012)

iii. New deep convection scheme improves Madden-Julian Oscillation in CCSM4

Subramanian et al. (2011) studied the impact of including the new convective momentum transport scheme and the dilute plume approximation in the ability of the CCSM4 to represent the Madden-Julian Oscillation (MJO). We used the US CLIVAR MJO Working Group prescribed diagnostic tests (Waliser et al., 2009) to evaluate the model's mean state, variance and wavenumber-frequency characteristics in a 20-year simulation of the intraseasonal variability in zonal winds at 850 hPa (U850) and 200 hPa (U200) and Outgoing Longwave Radiation (OLR). Unlike its predecessor, CCSM4 reproduces a number of aspects of MJO behavior, including its rainfall fields, more realistically.

CCSM4 produces coherent, broadbanded and energetic patterns in eastward propagating intraseasonal zonal winds and OLR in the tropical Indian and Pacific Oceans that are generally consistent with MJO characteristics (Fig. 5). Strong peaks occur in power spectra and coherence spectra with periods between 20-100 days and zonal wavenumbers between 1 and 3 (Fig. 6). Model MJO's, however, tend to be more broadbanded in frequency than in observations. Broadscale patterns, as revealed in combined EOFs of U850, U200 and OLR, are remarkably consistent with observations and indicate that large-scale convergence-convection coupling occurs in the simulated MJO.

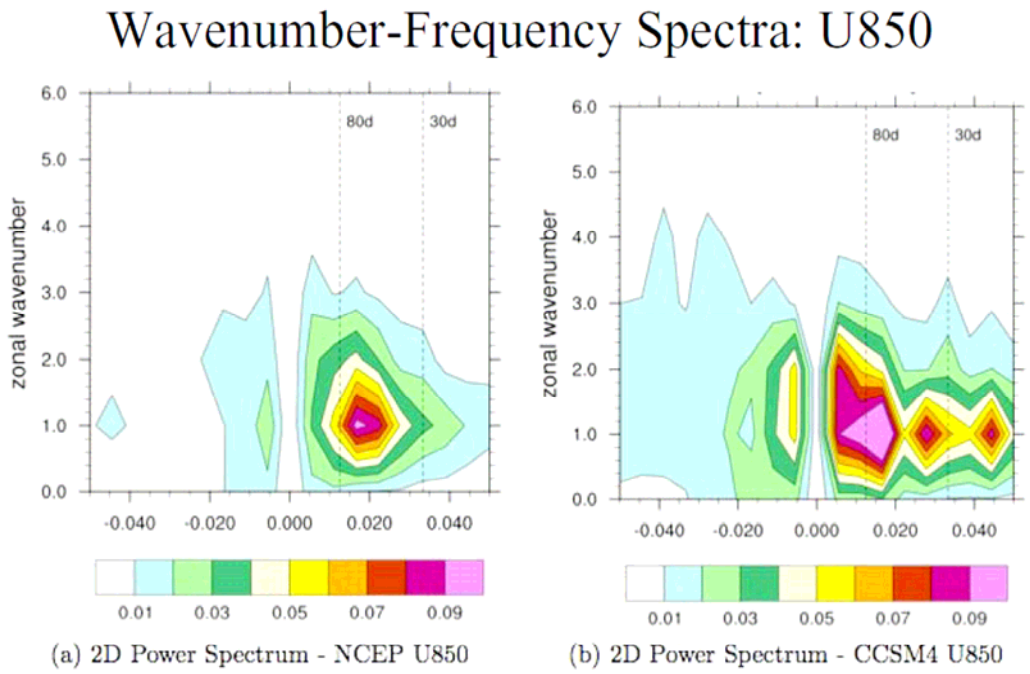

Figure 5. November-April wavenumber-frequency spectra of 10N-10S-averaged daily zonal 850 hPa winds of (a) NCEP (1981 - 2000) and (b) CCSM4 (20 years run). Individual spectra were calculated for each year, and then averaged over 20 years of data. Only the climatological seasonal cycle and time mean for each November-April segment were removed before calculation of the spectra. Units for the zonal wind spectrum are m^2/s^2 per frequency interval per wavenumber interval. The bandwidth is $(180\ days)^{-1}$. (From Subramanian et al., 2011)

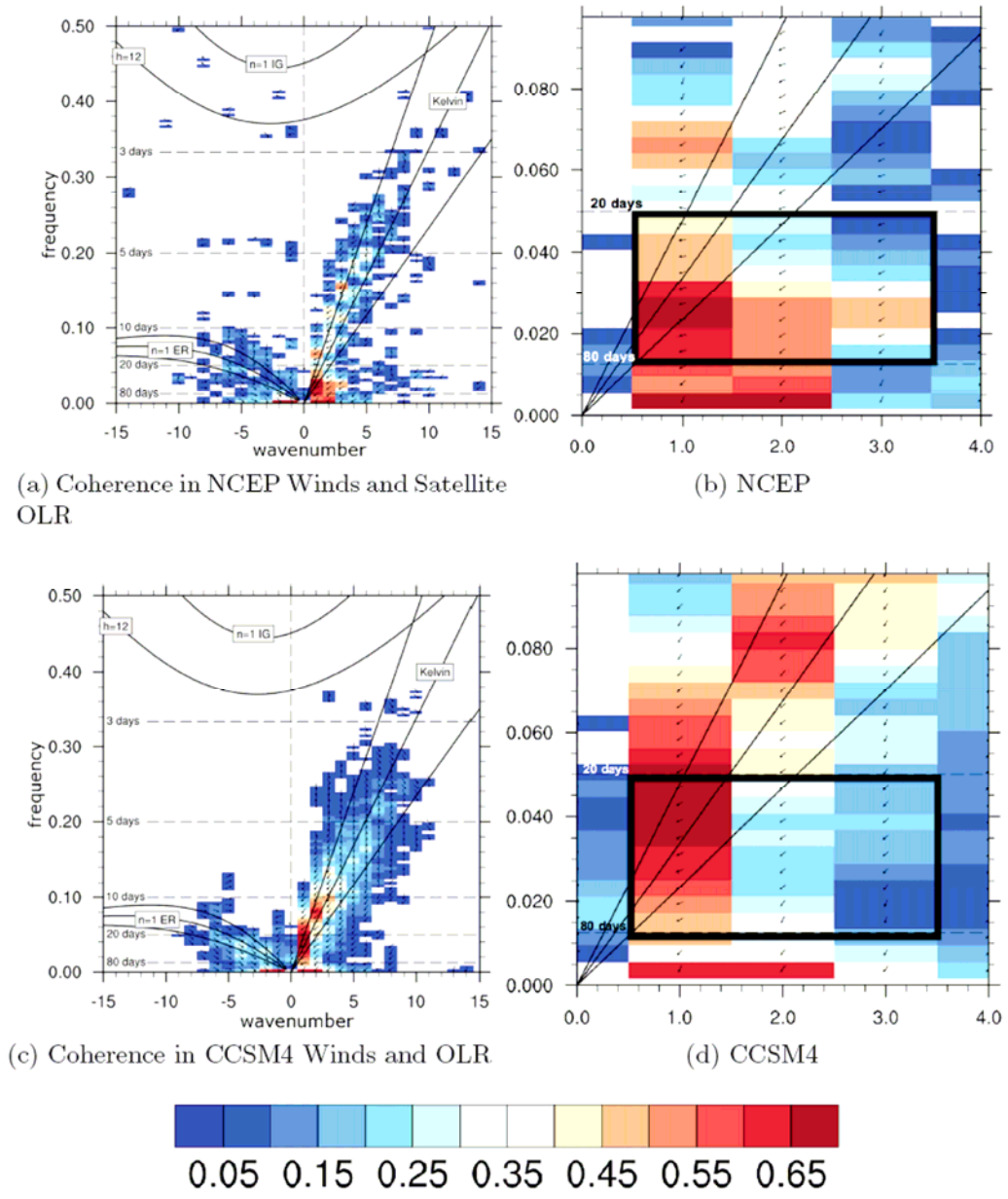

Figure 6. Coherence squared (colors) and phase lag (vectors) between zonal winds at 850 hPa winds and OLR are shown for (a) NCEP winds and satellite OLR (c) CCSM4 winds and OLR; (b) and (d) are expanded views of the MJO-relevant parts of the spectra. Only the symmetric spectra are shown here. Cross spectra are calculated using daily data during all seasons on 256-day-long segments, with consecutive segments overlapping by 206 days. Colors represent coherence squared between OLR and U850, and vectors represent the phase by which wind anomalies lag OLR anomalies, increasing in the clockwise direction. A phase of 0 is represented by a vector directed upward. Dispersion curves for the (n = -1) Kelvin, n = 1 equatorial Rossby (ER) and (n = 1) Inertia-Gravity waves corresponding to three equivalent depths (h = 12, 25, and 50 m) in the shallow water equations are overlaid (black contours). MJO is defined as the spectral components within zonal wavenumbers 1 to 3 and having periods 20 to 80 days as marked by the black box in the right panels. (From Subramanian et al., 2011)

Relations between MJO in the model and its concurrence with other climate states are also explored. MJO activity (defined as the percentage of time the MJO index exceeds 1.5) is enhanced during El Nino events compared to La Nina events both in the model and observations. MJO activity is increased during periods of anomalously strong negative meridional wind shear in the Asian Monsoon region, and also during strong negative Indian Ocean Zonal Mode states, in both the model and observations.

iv. Mesoscale SST anomalies affect precipitation in strong frontal regions

Putrasahan et al. (2012) consider the impact of strong SST anomalies on the atmospheric boundary layer, surface fluxes, and precipitation. We focus on the Kuroshio Extension region, which is characterized by energetic oceanic mesoscale and frontal variability that alters the air-sea fluxes that can influence large-scale climate variability in the North Pacific. We investigate this mesoscale air-sea coupling using a regional eddy-resolving coupled ocean-atmosphere (OA) model that downscales the observed large-scale climate variability from 2001-2007. The model simulates many aspects of the observed seasonal cycle of OA coupling strength for both momentum and turbulent heat fluxes.

We introduce a new modeling approach to study the scale-dependence of two well-known mechanisms for the surface wind response to mesoscale sea surface temperatures (SST), namely, the 'vertical mixing mechanism' (VMM) and the 'pressure adjustment mechanism' (PAM). We compare the fully coupled model to the same model with an online, 2-D spatial smoother applied to remove the mesoscale SST field felt by the atmosphere. Both VMM and PAM are found to be active during the strong wintertime peak as seen in the coupling strength from the model and observations. For VMM, large-scale SST gradients surprisingly generate coupling between downwind SST gradient and wind stress divergence that is often stronger than the coupling on the mesoscale, indicating their joint importance in OA interaction in this region. In contrast, VMM coupling between crosswind SST gradient and wind stress curl occurs only on the mesoscale, and not over large-scale SST gradients, indicating the essential role of the ocean mesocale. For PAM, the model results indicate that coupling between the Laplacian of sea level pressure and surface wind convergence occurs for both mesoscale and large-scale processes, but inclusion of the mesoscale roughly doubles the coupling strength. Coupling between latent heat flux and SST is found to be significant throughout the entire seasonal cycle in both fully-coupled mode and large-scale coupled mode, with peak coupling during winter months.

The atmospheric response to the oceanic mesoscale SST is studied by comparing the fully coupled run to an uncoupled atmospheric model forced with smoothed SST prescribed from the coupled run. Precipitation anomalies (Fig. 7) are found to be forced by surface wind convergence patterns that are driven by mesoscale SST gradients, indicating the importance of the ocean forcing the atmosphere at this scale. The response pentrates through the ABL in troposphere as indicated by the vertical velocity fields and rainfall fields.

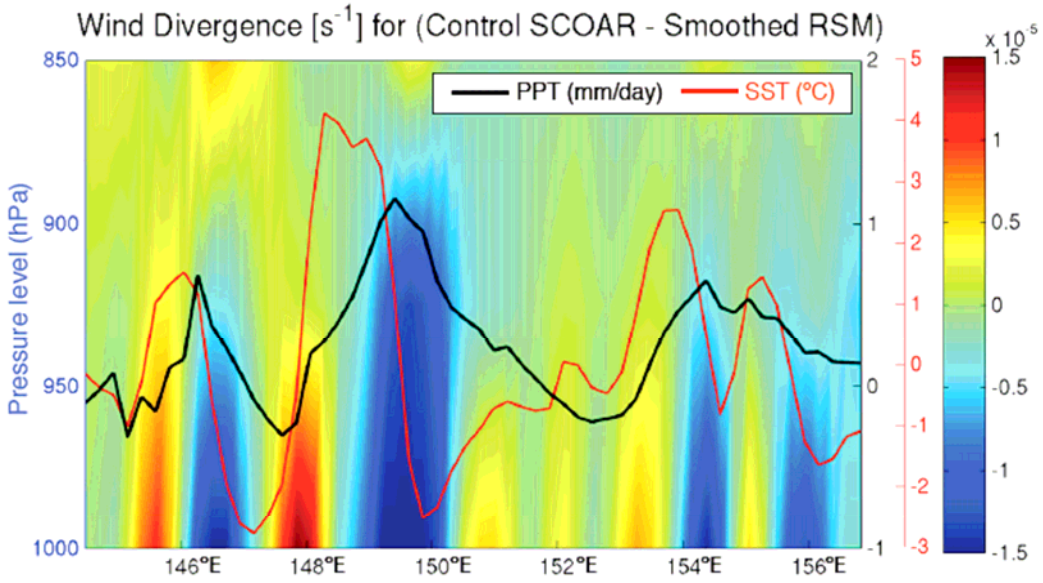

Figure 7: Vertical cross section of the difference in wind divergence (s^{-1}) from Control SCOAR - Smoothed RSM, at (144E to 156E, 40.5N) for January 2001. There is an overlay with SST difference (C; red) and precipitation difference (mm/day; black) from Control SCOAR.

b. Mentoring

Mr. Michael DeFlorio (Ph.D. defense expected in 2013) used global runs of CCSM to focus on California climate, and has presented his results at national meetings (AMS) and CCSM Workshops. **Mr. Nicholas Cavanaugh** (Ph.D. expected in 2014) developed statistical methods for detecting changes in statistics in global climate over time, which was inspired by his attending the NCAR 2011 Summer Colloquium on "*Statistical Assessment of Extreme Weather Phenomena Under Climate Change*".

Dr. Dian Putrasahan (Ph.D. 2012) developed a regional coupled ocean-atmosphere model of the precipitation response to mesoscale SST anomalies in the western North Pacific. She is now a post-doctoral researcher, with Drs. Lisa Beal and Ben Kirtman, at the University of Miami, working on coupled ocean-atmosphere modeling in the Algulhas Current System. **Dr. Aneesh Subramanian** (Ph.D. 2012) analyzed the precipiation processes associated with the Madden Julian Oscillation in CCSM4. He is now a post-doctoral researcher working with Dr. Guang Zhang (SIO) on tropical atmospheric convection parameterizations in NCAR's CESM.

c. Publications acknowledging this grant

DeFlorio, M. J., D. W. Pierce, D. R. Cayan and A. J. Miller, 2012: Western U.S. Extreme Precipitation Events and Their Relation to ENSO and the PDO in CCSM4. *Journal of Climate*, accepted pending revisions.

Pierce, D. W., D. R. Cayan, T. Das, E. P. Maurer, N. L. Miller, Y. Bao, M. Kanamitsu, K. Yoshimura, M. A. Snyder, L. C. Sloan, G. Franco, M. Tyree, 2012: The key role of heavy precipitation events in climate model disagreements of future annual precipitation changes in California. *Journal of Climate, sub judice.*

Putrasahan, D. A., A. J. Miller and H. Seo, 2012: Isolating mesoscale coupled ocean-atmosphere interactions in the Kuroshio Extension region. *Dynamics of Atmospheres and Oceans*, accepted pending revisions.

Subramanian, A. C., M. Jochum, A. J. Miller, R. Murtugudde, R. B. Neale and D. E. Waliser, 2011: The Madden Julian Oscillation in CCSM4. *Journal of Climate*, **24**, 6261-6282.